Composites Part B 168 (2019) 236–242

Contents lists available at ScienceDirect

Composites Part B

journal homepage: www.elsevier.com/locate/compositesb

Thermal-mechanical coupling buckling analysis of porous functionally graded sandwich beams based on physical neutral plane

Yijie Liu[a,1], Shengkai Su[a,b,1], Huaiwei Huang[b,*], Yingjing Liang[a]

[a] School of Civil Engineering, Guangzhou University, Guangzhou, 510006, PR China
[b] School of Civil Engineering and Transportation, South China University of Technology, Guangzhou, 510640, PR China

ARTICLE INFO

Keywords:
Functionally graded materials
Thermal buckling
Porosity
Iterative algorithm
Coupling

ABSTRACT

Porosity of functionally graded materials (FGMs) is usually aroused by fabrication defects. It had been proven that the porosity has a significant influence on the static responses of their structures, but the effects of porosity on buckling behaviors are still worth investigating. To reveal these effects, the thermal-mechanical coupling buckling issue of a clamped-clamped porous FGM sandwich beam is investigated in this paper by employing the high-order sinusoidal shear deformation theory. The modified Voigt mixture rule is used to approximate the temperature-dependent material properties of porous FGMs. The physical neutral plane of FGM sandwich beams is taken into account to reflect the actual condition of the structures and simplify the calculation. The thermal environments are considered as uniform, linear and nonlinear temperature rises, and both the temperature-independent and temperature-dependent material properties are discussed in order to justify the importance of the thermal-mechanical coupling effect. An iterative algorithm is used to solve the thermal-mechanical coupling critical buckling temperature. The present theoretical results are verified by comparing with the literature and ABAQUS results, and the effects of porosity, the physical neutral plane, gradient index, material temperature dependence, sandwich structural parameters are discussed. Results show that for buckling issue excluding the pre-buckling deformation effect, considering either the physical neutral plane or the geometrical middle plane of FGM beams would produce alike critical buckling temperatures. With the rise of porosity, the critical temperature increases greatly, which is quite different from the changing rule observed in the buckling issue of inplane-loaded porous FGM plates in literature. The beam with a smaller face-to-core ratio is more sensitive to the change in porosity. Moreover, to improve the thermal buckling load of FGM beams, ceramic constituents with the lower thermal expansion coefficient would be preferred.

1. Introduction

Functionally graded materials (FGMs) are a new kind of composites fabricated by mixing ceramic and metal constituents. As ideal heat-resistant materials, FGMs possess both the thermal resistance of the ceramic constituent and the crack-resistance of the metal constituent simultaneously. Controlling the volume fraction of the constituents in space domain would achieve their smooth gradient material properties, and thus excite their potential applications in optimizing thermodynamic performances of their structures, such as high-temperature and high-stress components in aircraft and automotive engineering fields [1].

Many studies focused on the thermal-mechanical coupling stability issues of FGM structures in the recent years. For example, Bouhadra et al. [2] studied the thermal buckling response of functionally graded plates subjected to uniform, linear and nonlinear temperature rises across the thickness direction. They found that for all the three thermal loading types, the thermal force resultant becomes larger as the ratio of metal-to-ceramic modules increases. Trinh et al. [3] investigated the thermal buckling of FGM beams under various thermal loads based on the state space approach. The results revealed that the critical temperatures under nonlinear temperature rise case are larger than those under linear temperature rise case, and the difference becomes more pronounced as the volume fraction index of ceramics increases. Besides, the solution considering the temperature-dependence of material properties gives significantly lower critical buckling temperatures than those with temperature-independence. Using a two-step perturbation method, She et al. [4] studied the thermal buckling and postbuckling of

* Corresponding author.
E-mail address: cthwhuang@scut.edu.cn (H. Huang).
[1] These authors contributed equally to this work.

https://doi.org/10.1016/j.compositesb.2018.12.063
Received 11 August 2018; Received in revised form 7 December 2018; Accepted 14 December 2018
Available online 19 December 2018
1359-8368/

clamped-clamped FGM beams subjected to uniform temperature rise. The results indicated that the thermal post-buckling equilibrium paths for FGM beams are stable, and the thermal post-buckling response of FGM beams under temperature-dependent case is lower than that under temperature-independent case.

However, due to the great difference in the solidification temperatures between the ceramic and metal constituents, FGMs may have some micro-voids during the sintering preparation [5]. Wattanasakulpong et al. [6] also found the similar porous phenomenon of FGMs in multi-step continuous infiltration process. Investigations on the effects of porosity were addressed mainly for vibration characteristics of porous FGM beams [7–11], in which the modified Voigt mixing rule was used to approximate the material properties. The results indicated that porosity may lead to a great decrease in vibration frequencies. For buckling issues, Atmane et al. [12] and Barati et al. [13] presented the buckling analysis for in-plane compressed porous FGM beams and plates resting on an elastic foundation. It was proven that the critical buckling load is inversely proportional to the value of porosity, and considering the uniform porosity distribution in FGMs would give a smaller critical buckling load than the non-uniform distribution.

Besides, most of the aforementioned literature established their theories based on the geometrical middle plane. But due to the asymmetry of material properties of FGMs with respect to the geometrical middle plane, the stretching and bending equations are coupled. With the physical neutral plane concept, Zhang [14] and Abrate [15] have shown that if the reference plane is properly selected, there is no stretching-bending coupling in constitutive equations. Prakash et al. [16] studied the effect considering physical neutral plane on the nonlinear stability behavior of FGM plates under compression. It is found that the post-buckling path of FGM plates would be quite different when the physical neutral plane is taken into account. However, with an efficient sinusoidal shear deformation theory and the physical neutral plane concept, Bouiadjra et al. [17] investigated the thermal buckling behavior of FGM plates and the results have a good agreement with those based on the geometrical middle plane. Also, Bellifa et al. [18] presented bending and free vibration analysis of FGM plates using a simple first-order shear deformation theory based on the exact position of the physical neutral plane, and the results are identical to those of the conventional first-order shear deformation theory. Moreover, more and more researches have been attached to investigate the effects of the physical neutral plane in bending, free vibration, nonlinear vibration issues of FGM structures in the recent years [19–25].

To the author's best knowledge, there is no investigation on the thermal-mechanical coupling buckling behaviors of porous FGM beams, especially for porous FGM sandwich beams. In this paper, thermal-mechanical coupling buckling issue of clamped-clamped porous FGM sandwich beams is investigated by employing the high-order sinusoidal shear deformation theory (SSDT). The modified Voigt mixture rule with porosity is used to approximate the temperature-dependence material properties of porous FGMs and the physical neutral plane of FGM beams is taken into account. The thermal environments are considered being uniform, linear and nonlinear temperature rises. Both temperature-independent and temperature-dependent material properties are examined. Finally, an iterative algorithm is used to solve the thermal-mechanical coupling critical buckling temperature.

2. Porous FGM sandwich beams

Consider a clamped-clamped porous FGM beam with length L and width b and height $h = h_f + 2h_a$ as shown in Fig. 1. It is supposed that the displacement of the beam between the layers is continuous. The top and bottom layer of the sandwich beam are respectively made of homogeneous ceramic and metal constituents with the height h_a, while the core layer is made of FGMs with the height h_f. By setting $k = 1,2,3$ to denote the top, core and bottom layer of FGM beams, respectively. And we have the volume fraction of ceramic constituents $V_c^{(k)}$ in the FGM

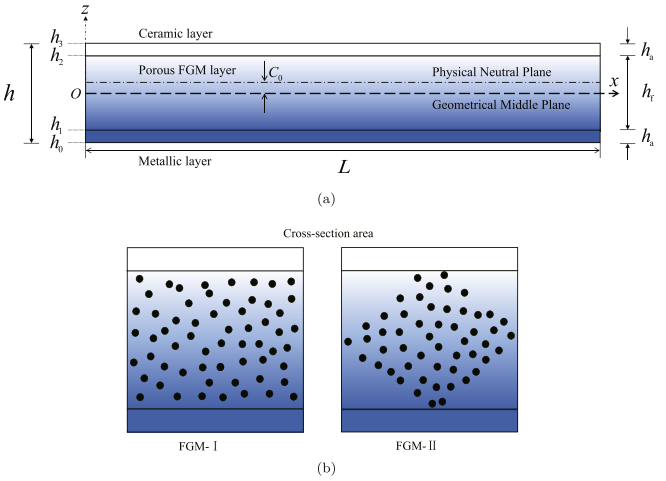

Fig. 1. Geometry of a clamped-clamped porous FGM sandwich beam.

core layer

$$V_c^{(1)}(z) = 1, \quad V_c^{(2)}(z) = \left(\frac{z}{h_f} + \frac{1}{2}\right)^n, \quad V_c^{(3)}(z) = 0, \quad V_c^{(k)}(z) + V_m^{(k)}(z) = 1 \tag{1}$$

where the subscript c,m denote the ceramic and metal constituents respectively and n is the power-law index indicating the inhomogeneity of FGMs.

Additionally, according to the principle of the multi-step sequential infiltration technique that can be employed to fabricate FGM samples [6], the porosities mostly occur at the middle zone due to different infiltration process. Thus, two types of porosity distributions in core named as FGM-I and FGM-II are discussed. For FGM-I, the porosity phases distribute uniformly over the cross section, while for FGM-II, the porosity phase distributes around the mid-zone of the cross-section in a rhombus shape, as shown in Fig. 1 (b). With the modified Voigt mixing rule proposed by Wattanasakulpong et al. [8], the effective material properties of FGMs $P(z)$ representing the Young's modulus $E(z)$, thermal expansion coefficient $\alpha(z)$ and thermal conductivity $\kappa(z)$ can be approximated as

$$P^{(2)}(z) = (P_c - P_m)\left(\frac{1}{2} + \frac{z}{h_f}\right)^n + P_m - \zeta\frac{\beta}{2}(P_c + P_m) \tag{2}$$

where $\beta(\beta \ll 1)$ denotes the volume fraction of porosity, distributed equally in the ceramic and metal phases. And we have $\zeta = 1$ for FGM-I and $\zeta = 1 - 2|z|/h_f$ for FGM-II.

It is clear that the effective material properties decrease with the increase of porosity for both FGM-I and FGM-II. Meanwhile, the material properties should be temperature-dependent and can be expressed as

$$P_i = c_0(c_{-1}T_{-1} + 1 + c_1T + c_2T^2 + c_3T^3) \tag{3}$$

where $i =$ c, m. T is temperature in Kelvin, and $c_j(j = -1,0,1,2,3)$ are the material temperature coefficients [3,26] listed in Table 1. The temperature-dependent material properties are also illustrated in Fig. 2. The Poisson's ratio of FGMs is assumed to be constant, i.e. $\nu = (\nu_c + \nu_m)/2$ evaluated at $T = 300$K.

3. Theory and formulation

3.1. Basic formulations

The position of the physical neutral plane ($z = C_0$) satisfies the following relation.

Table 1
Temperature-dependent coefficients for ceramic and metals [3,26].

Constituents	Properties	c_0	c_1	c_2	c_3
Si_3N_4	E(Pa)	348.43×10^9	-3.070×10^{-4}	2.160×10^{-7}	-8.946×10^{-11}
	α(1/K)	5.8723×10^{-6}	9.095×10^{-4}	0	0
	κ(W/mK)	13.723	-1.032×10^{-3}	5.466×10^{-7}	-7.876×10^{-11}
	ν	0.2400	0	0	0
ZrO_2	E(Pa)	244.27×10^9	-1.371×10^{-3}	1.214×10^{-6}	-3.681×10^{-10}
	α(1/K)	12.766×10^{-6}	-1.491×10^{-3}	1.006×10^{-5}	-6.778×10^{-11}
	κ(W/mK)	1.7	1.276×10^{-4}	6.648×10^{-8}	0
	ν	0.2882	1.133×10^{-4}	0	0
SUS304	E(Pa)	201.04×10^9	3.079×10^{-4}	-6.534×10^{-7}	0
	α(1/K)	12.330×10^{-6}	8.086×10^{-4}	0	0
	κ(W/mK)	15.379	-1.264×10^{-3}	2.092×10^{-6}	-7.223×10^{-10}
	ν	0.3262	-2.002×10^{-4}	3.797×10^{-7}	0

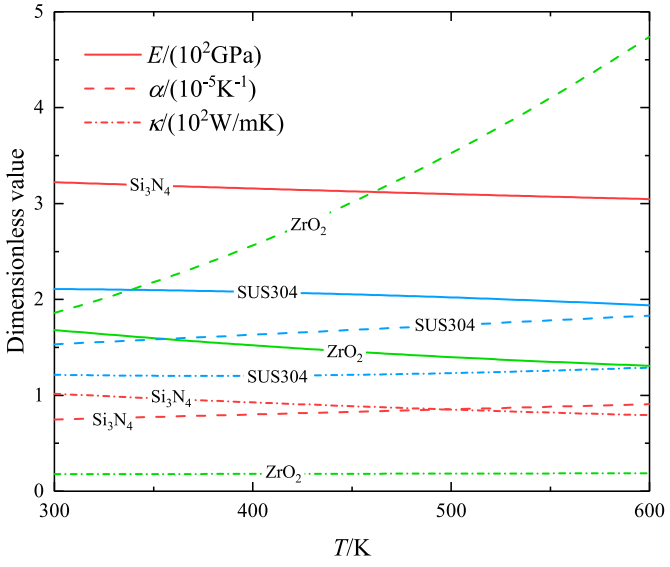

Fig. 2. Material properties of constituents with respect to temperature change.

$$C_0 = \frac{\int_{h_{k-1}}^{h_k} zE^{(k)}(z,\,T)\mathrm{d}z}{\int_{h_{k-1}}^{h_k} E^{(k)}(z,\,T)\mathrm{d}z}, \quad C_1 = \frac{\int_{h_{k-1}}^{h_k} \psi(z)E^{(k)}(z,\,T)\mathrm{d}z}{\int_{h_{k-1}}^{h_k} E^{(k)}(z,\,T)\mathrm{d}z} \tag{4}$$

where C_0 is equal to 0 for homogeneous isotropic beams. As shown in Fig. 3, it is worth noting that C_0 and C_1 are also temperature-dependent, so the physical neutral plane would vary with thermal environments. The displacements u_x and u_z of the beam in the x and z directions could be given by

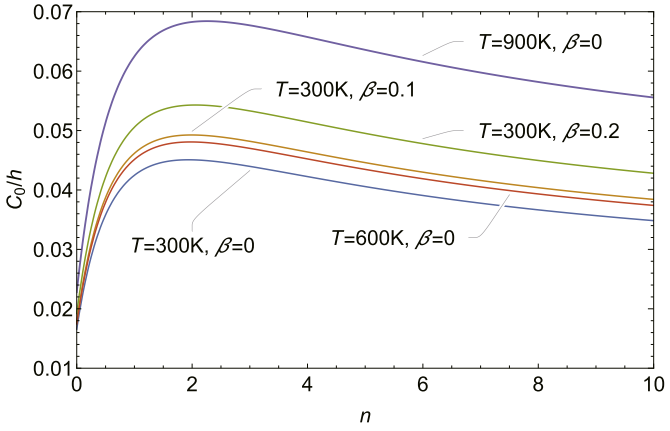

Fig. 3. Flowchart of iterative solution for TD case.

$$u_x(x,\,z) = u_0(x) - (z - C_0)\omega_0'(x) + [\psi(z) - C_1]\,\varphi_0(x), \quad u_z(x,\,z) = \omega_0(x) \tag{5}$$

where $u_0(x)$ and $w_0(x)$ are the axial displacement and deflection on the geometrical middle plane, respectively. $\varphi_0(x)$ is the rotation angle about the x-axes. $\psi(z)$ denotes the shape function determining the distribution of transverse shear strain and stress along the thickness. We have its form in SSDT [27], the first-order shear deformation theory (FSDT) and the classical shear deformation theory (CSDT) as

$$\psi(z) = \begin{cases} \frac{h}{\pi}\sin\left[\frac{\pi(z)}{h}\right] & \text{SSDT} \\ z & \text{FSDT} \\ 0 & \text{CSDT} \end{cases} \tag{6}$$

Under the framework of small deformation, the strain components can be expressed as

$$\varepsilon_{xx} = u_0'(x) - (z - C_0)\omega_0''(x) + [\psi(z) - C_1]\varphi_0'(x), \quad \gamma_{xz} = \varphi_0(x)\psi'(z) \tag{7}$$

So the stress components in the k layer are obtained as

$$\sigma_{xx}^{(k)} = E^{(k)}\varepsilon_{xx}, \quad \tau_{xz}^{(k)} = \frac{E^{(k)}}{2(1+\nu)}\gamma_{xz}, \quad \sigma_{xx}^{\mathrm{T}(k)} = -E^{(k)}\alpha^{(k)}\Delta T \tag{8}$$

where $\Delta T = T - T_0$ and T_0 is the initial temperature.

3.2. Buckling analysis

The strain energy U and the potential energy V due to thermal stress can be expressed as

$$U = \frac{1}{2}b\int_0^L \sum_{k=1}^{3}\int_{h_{k-1}}^{h_k} (\sigma_{xx}^{(k)}\varepsilon_{xx} + \tau_{xz}^{(k)}\gamma_{xz})\mathrm{d}z\mathrm{d}x \tag{9}$$

$$V = \frac{1}{2}b\int_0^L \sum_{k=1}^{3}\int_{h_{k-1}}^{h_k} \sigma_{xx}^{\mathrm{T}(k)}\omega_0''(x)\mathrm{d}z\mathrm{d}x \tag{10}$$

Applying Hamilton principle $\delta\,\Pi = \delta(U + V) = 0$ yields

$$\begin{aligned}
&\textstyle\sum_{k=1}^{3}\int_{h_{k-1}}^{h_k} E^{(k)}\{u_0''(x) - (z - C_0)\omega_0'''(x) + [\psi(z) - C_1]\,\varphi_0''(x)\}\mathrm{d}z = 0 \\
&\textstyle\sum_{k=1}^{3}\int_{h_{k-1}}^{h_k} E^{(k)}(z - C_0)\{u_0'''(x) - (z - C_0)\omega_0''''(x) \\
&\quad + [\psi(z) - C_1]\varphi_0'''(x)\}\mathrm{d}z \\
&+ \omega_0''(x)\textstyle\sum_{k=1}^{3}\int_{h_{k-1}}^{h_k} -E^{(k)}\alpha^{(k)}\Delta T\mathrm{d}z = 0 \\
&\textstyle\sum_{k=1}^{3}\int_{h_{k-1}}^{h_k} E^{(k)}[\psi(z) - C_1]\{u_0'''(x) - (z - C_0)\omega_0'''(x) \\
&\quad + [\psi(z) - C_1]\varphi_0'''(x)\}\mathrm{d}z = 0 \\
&-\textstyle\sum_{k=1}^{3}\int_{h_{k-1}}^{h_k} \frac{E^{(k)}}{2(1+\nu)}\varphi_0(x)[\psi'(z)]^2\mathrm{d}z
\end{aligned} \tag{11}$$

For clamped-clamped sandwich FGM beams, the boundary conditions are

$$u_0(x) = \omega_0(x) = \omega_0{}'(x) = \varphi_0(x) = 0, \quad \text{at } x = 0, L$$

Here, to satisfy the boundary conditions, the displacement components are assumed as [2,4].

$$\begin{cases} u_0(x) & = \sum_{m=1}^{\infty} \xi_u \sin(\lambda x)\cos(\lambda x) \\ \omega_0(x) & = \sum_{m=1}^{\infty} \xi_\omega \sin(\lambda x)\sin(\lambda x) \\ \varphi_0(x) & = \sum_{m=1}^{\infty} \xi_\varphi \sin(\lambda x)\cos(\lambda x) \end{cases} \tag{12}$$

where $\lambda = m\pi/L$, and $\xi_j (j = u, \omega, \varphi)$ are the unknown amplitudes.

Substituting Eq. (12) into Eq. (11), the generalized eigenvalue problem for thermal buckling can be written as

$$\{[K] + [K^{\mathrm{T}}]\}\{\Lambda\} = 0 \tag{13}$$

where $\{\Lambda\} = \{\xi_u, \xi_\omega, \xi_\varphi\}^T$ and $[K]$ and $[K^{\mathrm{T}}]$ can be defined as

$$[K] = \begin{bmatrix} 4\lambda^2 A_{11} & -8\lambda^3 B_{11} & 4\lambda^2 C_{11} \\ -8\lambda^3 B_{11} & 16\lambda^4 D_{11} & -8\lambda^3 F_{11} \\ 4\lambda^2 C_{11} & -8\lambda^3 F_{11} & 4\lambda^2 H_{11} + A_{55} \end{bmatrix}, \quad [K^{\mathrm{T}}] = \begin{bmatrix} 0 & 0 & 0 \\ 0 & 4\lambda^2 N^{\mathrm{T}} & 0 \\ 0 & 0 & 0 \end{bmatrix}$$

$$\begin{aligned} \{A_{11}, B_{11}, D_{11}\} &= \sum_{k=1}^{3} \int_{h_{k-1}}^{h_k} E^{(k)} \{1, z - C_0, (z - C_0)^2\} \mathrm{d}z \\ \{C_{11}, F_{11}, H_{11}\} &= \sum_{k=1}^{3} \int_{h_{k-1}}^{h_k} E^{(k)} \\ &\quad \{\psi(z) - C_1, (z - C_0)[\psi(z) - C_1], [\psi(z) - C_1]^2\} \mathrm{d}z \\ A_{55} &= \sum_{k=1}^{3} \int_{h_{k-1}}^{h_k} \frac{E^{(k)}}{2(1+\nu)} [\psi'(z)]^2 \mathrm{d}z \\ N^{\mathrm{T}} &= \sum_{k=1}^{3} \int_{h_{k-1}}^{h_k} -E^{(k)} \alpha^{(k)} (T - T_0) \mathrm{d}z \end{aligned} \tag{14}$$

Additionally, it is worth mentioning that the stretching-bending coupling effect would disappear after introducing the physical neutral plane concept, which leads to $B_{11} = C_{11} = 0$ in Eq. (14), so that the calculation can be simplified.

4. Thermal environments

Assume the FGM beams are exposed to thermal environments, including uniform temperature rise (UTR), linear temperature rise (LTR) and nonlinear temperature rise (NLTR).

For UTR, the temperature rises ΔT from the initial temperature $T_0 = 300\mathrm{K}$ to the temperature T, so the temperature field can be expressed as

$$T = T_0 + \Delta T \tag{15}$$

For LTR, the temperature field distributes linearly from the top surface T_c to the bottom surface $T_m = 300\mathrm{K}$, through the thickness, and it can be expressed as

$$T(z) = T_m + (T_c - T_m)\left(\frac{1}{2} + \frac{z}{h}\right) \tag{16}$$

For NLTR, the temperature field distributes nonlinearly from the top surface T_c to the bottom surface $T_m = 300\mathrm{K}$. In this case, the one-dimensional steady-state heat conduction through the thickness is considered, i.e.

$$-\frac{\mathrm{d}}{\mathrm{d}z}\left[\kappa^{(k)}(z)\frac{\mathrm{d}T(z)}{\mathrm{d}z}\right] = 0 \tag{17}$$

Taking into account the thermal continuous conditions between different layers yields

$$\begin{cases} T^{(1)}(z) = T_1 + (T_c - T_1)\left[\frac{1}{2} + \frac{2z - (h_f + h_a)}{2h_a}\right], & \frac{h_f}{2} < z < h_a + \frac{h_f}{2} \\ T^{(2)}(z) = T_2 + (T_1 - T_2)\frac{\int_{-h_f/2}^{z} \frac{1}{\kappa^{(2)}(z)} \mathrm{d}z}{\int_{-h_f/2}^{h_f/2} \frac{1}{\kappa^{(2)}(z)} \mathrm{d}z}, & -\frac{h_f}{2} < z < \frac{h_f}{2} \\ T^{(3)}(z) = T_m + (T_2 - T_m)\left[\frac{1}{2} + \frac{2z + (h_f + h_a)}{2h_a}\right], & -h_a - \frac{h_f}{2} < z < -\frac{h_f}{2} \end{cases} \tag{18}$$

where

$$T_1 = T_c - (T_c - T_m)\frac{h_a \mu_2}{(\mu_1 + \mu_2)h_a + \mu_1 \mu_2 \int_{-h_f/2}^{h_f/2} \frac{1}{\kappa^{(2)}(z)} \mathrm{d}z}$$

$$T_2 = T_m + (T_c - T_m)\frac{h_a \mu_1}{(\mu_1 + \mu_2)h_a + \mu_1 \mu_2 \int_{-h_f/2}^{h_f/2} \frac{1}{\kappa^{(2)}(z)} \mathrm{d}z}$$

$$\mu_1 = \kappa_c - (\kappa_c + \kappa_m)\beta/2, \quad \mu_2 = \kappa_m - (\kappa_c + \kappa_m)\beta/2$$

In the case of FGM-I, Eq. (18) can be solved by using an approximation of polynomial series expansion.

$$\begin{cases} T^{(1)}(z) = \widehat{T_1} + (T_c - \widehat{T_1})\left[\frac{1}{2} + \frac{2z - (h_f + h_a)}{2h_a}\right], & \frac{h_f}{2} < z < h_a + \frac{h_f}{2} \\ T^{(2)}(z) = \widehat{T_2} + (\widehat{T_1} - \widehat{T_2})\frac{D_1(z)}{D_0(z)}, & -\frac{h_f}{2} < z < \frac{h_f}{2} \\ T^{(3)}(z) = T_m + (\widehat{T_2} - T_m)\left[\frac{1}{2} + \frac{2z + (h_f + h_a)}{2h_a}\right], & -h_a - \frac{h_f}{2} < z < -\frac{h_f}{2} \end{cases} \tag{19}$$

where

$$\widehat{T_1} = T_c - (T_c - T_m)\frac{\vartheta h_a}{h_f D_0(z) + (\vartheta + 1)h_a}$$

$$\widehat{T_2} = T_m + (T_c - T_m)\frac{h_a}{h_f D_0(z) + (\vartheta + 1)h_a}$$

$$\vartheta = \sum_{i=0}^{r} \left(\frac{\kappa_m - \kappa_c}{\kappa_m - (\kappa_c + \kappa_m)\frac{\beta}{2}}\right)^i$$

$$D_j(z) = \sum_{i=0}^{r} \left(\frac{\kappa_m - \kappa_c}{\kappa_m - (\kappa_c + \kappa_m)\frac{\beta}{2}}\right)^i \frac{[1/2 + z/h_f]^{(in+1)j}}{in + 1}, \ (j = 0,1)$$

where r denotes the item numbers of the series and $r = 5$ is chosen to satisfy the calculation precision.

To examine the temperature dependence effect of material properties on thermal buckling of porous sandwich beams, a comparison will be made between the temperature-dependence (TD) and temperature-independence (TID) cases. For TD case, the thermal-mechanical coupling buckling solution is solved by the iterative procedure as shown in Fig. 4. The determinant of the coefficient matrix in Eq. (13) must vanish to ensure non-zero solution, giving $[K] + [K^{\mathrm{T}}] = 0$. Specially, the critical buckling temperature $\Delta T_{cr} = T - T_0$ under UTR can be solved analytically as

$$T_{cr} = \frac{16\lambda^4(F_{11}^2 - D_{11}H_{11}) - 4\lambda^2 A_{55} D_{11}}{(A_{55} + 4H_{11}\lambda^2)\Gamma} \tag{20}$$

where

$$\Gamma = \sum_{k=1}^{3} \int_{h_{k-1}}^{h_k} -E^{(k)} \alpha^{(k)} \mathrm{d}z$$

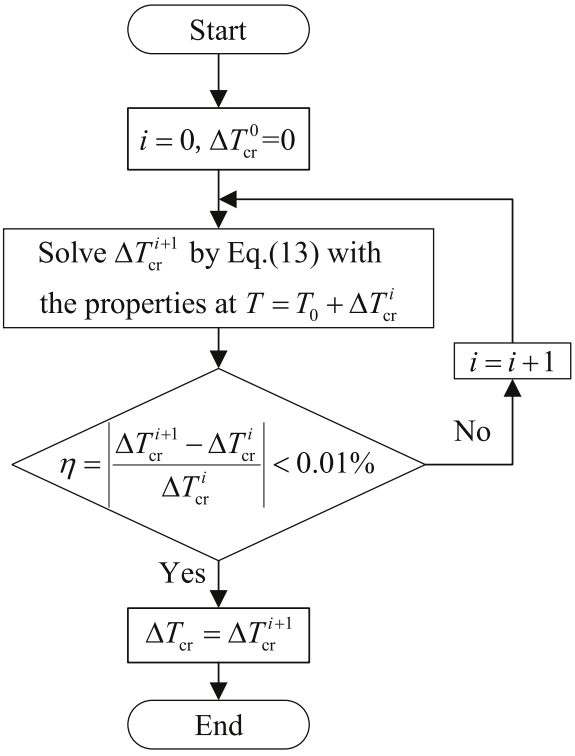

Fig. 4. Flowchart of iterative solution for TD case.

5. Theoretical verification and result analyses

5.1. Comparison study

To verify the present theory, comparisons are made for perfect FGM beams and perfect sandwich FGM beams subjected to UTR thermal environment. Setting $h_a = 0$ would degenerate the sandwich beam into a single FGM layer. From Table 2, the comparison study indicates the critical buckling temperatures, predicted by the present formulation based on physical neutral plane, are in agreement with the theoretical results of Ref. [4,28] under both TID and TD cases and the deviations are within 0.1%. For perfect sandwich FGM beams without porosity, an ABAQUS finite element model was built to verify the present theory. As the aforementioned, FGMs can be seen as laminated structures with multiple composite layers. For modeling such a laminated structure, the Composite Layups tools in ABAQUS is used to create a conventional shell with 50 layers. Each layer is homogeneous and has the same thickness, but the material properties of the laminated structure vary spatially in a gradient. Here the element type is S8R and the Lanczos method in the linear perturbation buckle step is used to solve the critical temperatures. Table 3 indicates a maximum deviation of 0.3% between the present theoretical predictions and those by ABAQUS. Tables 2 and 3 also reveal that the critical temperatures predicted in the geometrical middle plane (GMP) and the physical neutral plane (PNP) cases are nearly equal to each other, which is consistent with the results in Ref. [17]. Therefore, the following theoretical results will be produced by the formulation based on PNP.

Table 2
Verification of the critical temperature (in K) of FGM beams ($L/h = 25$, $\beta = 0$, UTR).

Cases	Sources	$n = 0.5$	$n = 1$	$n = 2$	$n = 5$	$n = 10$
TID	Ref. [28]	509.890	458.680	423.530	394.390	376.140
	Ref. [4]	510.002	458.780	423.624	394.488	376.223
	Present (GMP)	510.189	458.904	423.629	394.393	376.191
	Present (PNP)	510.189	458.904	423.629	394.393	376.191
TD	Ref. [28]	399.500	367.320	345.150	326.400	313.580
	Ref. [4]	399.571	367.388	345.218	326.462	313.648
	Present (GMP)	399.694	367.470	345.213	326.380	313.617
	Present (PNP)	399.694	367.470	345.213	326.380	313.617

Table 3
Verification of the critical temperature (in K) of sandwich Si_3N_4/SUS304 FGM beams ($L/h = 50$, TID).

h_a/h_f	N	ABAQUS	Present	
			SSDT, PNP	SSDT, GMP
0.125	0.2	137.070	137.121	137.121
	1	116.460	116.556	116.556
	5	106.120	106.205	106.205
0.5	0.2	126.590	126.932	126.932
	1	117.350	117.447	117.447
	5	112.580	112.638	112.638

Table 4
Effects of slenderness ratio on the critical temperature (in K) of sandwich FGM-I ($n = 1$) beams under different thermal environments (TID).

L/h	β	$h_a/h_f = 0.125$			$h_a/h_f = 0.5$		
		SSDT	FSDT	CSDT	SSDT	FSDT	CSDT
UTR							
30	0	321.520	321.577	325.045	323.997	324.049	327.516
	0.1	360.756	360.860	364.861	354.512	354.685	358.622
	0.2	407.968	408.149	412.819	387.439	387.792	392.268
50	0	116.556	116.564	117.016	117.447	117.453	117.906
	0.1	130.814	130.828	131.350	128.567	128.590	129.104
	0.2	147.981	148.005	148.615	140.586	140.632	141.217
LTR							
30	0	678.490	678.610	685.930	690.703	690.814	698.206
	0.1	766.466	766.687	775.188	760.309	760.679	769.124
	0.2	873.955	874.343	873.955	836.358	837.119	836.358
50	0	245.964	245.980	246.935	250.375	250.390	251.354
	0.1	277.929	277.958	279.068	275.734	275.782	276.885
	0.2	317.008	317.059	317.008	303.480	303.580	303.480
NLTR							
30	0	712.988	713.114	720.806	732.405	732.523	740.361
	0.1	808.863	809.097	818.068	809.345	809.739	818.728
	0.2	926.767	927.178	937.787	894.299	895.113	905.446
50	0	258.470	258.486	259.490	265.492	265.507	266.530
	0.1	293.303	293.334	294.504	293.517	293.569	294.742
	0.2	336.164	336.219	337.603	324.504	324.612	325.961

From Table 4, the critical temperatures of Si_3N_4/SUS304 FGM-I sandwich beams predicted by SSDT and FSDT (the shear correct factor is $\frac{10(1+\upsilon)}{12+11\upsilon}$) are slightly smaller than those of CSDT. The deviations are within 1.2%. Meanwhile, with the increasing value of the h_a/h_f and L/h, the critical temperature T_{cr} decreases greatly. However, it is interesting that T_{cr} would rise as the porosity parameter increases. For instances, when the porosity increases by 0.1, the critical temperature increases by 9–15% for the beams with $h_a/h_f = 0.125$.

5.2. Thermal buckling under UTR

In the following parts, SSDT is used to calculate the theoretical results and all the calculation parameters are given in the figures for brevity. Fig. 5 gives the changing rules of the critical temperature with the power-law index and porosity parameter. Fig. 5 (a) and (b) are plotted for Si_3N_4/SUS304 and ZrO_2/SUS304 FGMs, respectively. T_{cr} decreases monotonically with the rising value of n for Si_3N_4/SUS304 FGMs, but increases for ZrO_2/SUS304 FGMs. Meanwhile, these curves would tend to be a steady value in a large value of n. It means that, for ZrO_2/SUS304 FGMs, the existence of the ceramic constituent would reduce the critical temperature, rather than increasing the thermal resistance of structures. So it is confirmed that to improve the critical

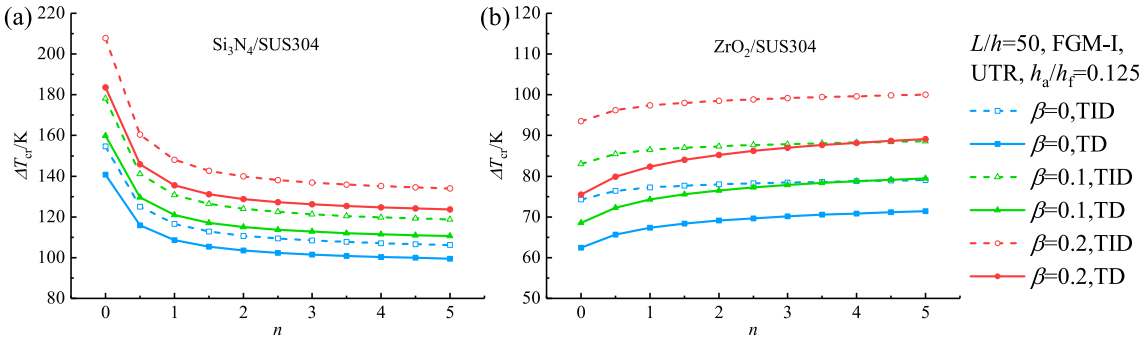

Fig. 5. Effects of the porosity and power-law index on thermal buckling of sandwich FGM-I beams under UTR.

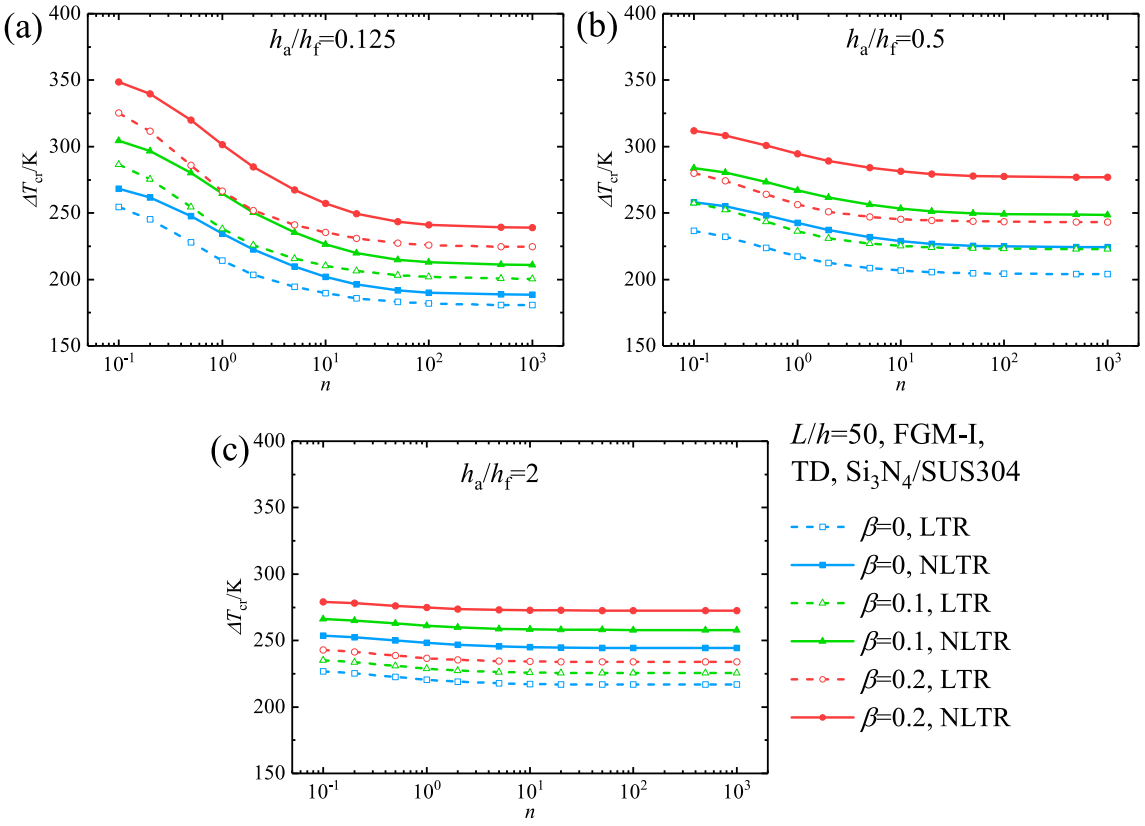

Fig. 6. Effects of the porosity and power-law index on thermal buckling of sandwich FGM-I beams under LTR and NLTR.

temperature, the ceramic constituent ZrO_2 is unsuitable to mix with SUS304. This is caused by its large thermal expansion coefficient relative to other ceramic constituents as witnessed in Fig. 2. Therefore, to improve the thermal buckling load of FGM beams, ceramic constituents with lower thermal expansion coefficients would be preferred.

Besides, the TID results are approximately 6–25% higher than those of TD, which indicates that neglecting the temperature-dependence of the constituent would overestimate the actual critical temperature. Meanwhile, from both figures, it is interesting that the existence of the porosity would heighten the overall curves of critical buckling temperatures. This result is quite different from the changing rule of the critical buckling mechanical load of porous FGM plates obtained in Refs. [12,13]. In fact, it is not paradoxical because porosity would decrease the Young's modulus and the thermal expansion coefficient of FGMs synchronously. Reduction in the latter would certainly decrease the load induced by temperature rise before thermal buckling.

5.3. Thermal buckling analyses under LTR and NLTR

Practically, FGMs are usually served for thermal barrier environments with temperature gradients, where temperature-dependent material properties of FGMs should be considered as the aforementioned. To focus on the temperature gradient effects, both LTR and NLTR are discussed in this part. Fig. 6 illustrates the critical temperature changing with the porosity parameter and the power-law index of Si_3N_4/SUS304 FGMs with TD material properties. Similar to Fig. 5(a), T_{cr} decreases monotonically with the rising value of n.

It is worth noting that there are significant differences between the LTR and the NLTR case, and the latter includes the practical thermal conduction effect. The NLTR results are higher by 4–17% than those of LTR. This illustrates that, as a simplified method of thermal environment, LTR would arouse tremendous error and greatly underestimate the critical buckling temperature. Besides, comparing Fig. 6 (a) and (b) indicates that the critical temperature of the sandwich beam with a smaller face-to-core ratio h_a/h_f is more sensitive to the change of the power-law index and the porosity parameter.

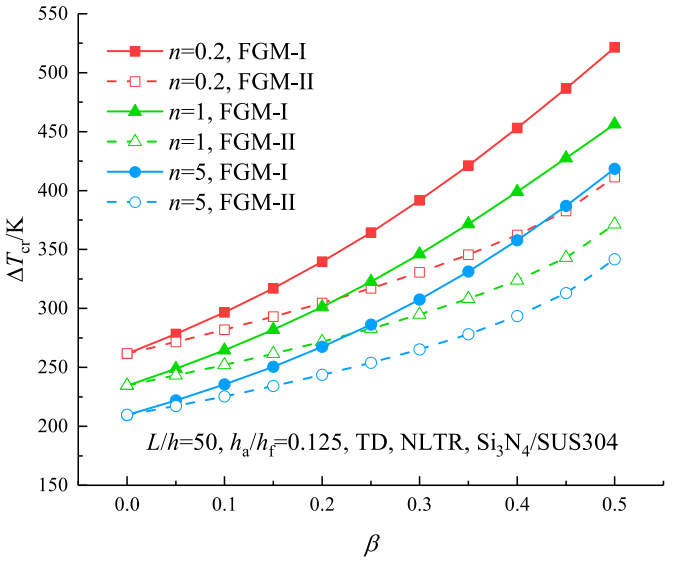

Fig. 7. Porosity effects on thermal buckling of sandwich FGM beams under NLTR.

5.4. Porosity effects

To further reveal the effects of porosity on thermal buckling of sandwich FGM beams in the practical conditions, by considering the TD and NLTR cases, comparisons are made between different porosity distributions including the FGM-I and FGM-II cases as shown in Fig. 7. In both cases, T_{cr} increases with the rising value of the porosity parameter, which is similar to the aforementioned. The critical buckling temperatures in the FGM-I case are larger than those in the FGM-II case and the deviations enlarge gradually as the porosity increases. Hence, in the FGM-I case, porosity effects more significantly on the critical temperatures of FGM sandwich beams than in the FGM-II case.

6. Conclusion

Thermal-mechanical coupling buckling behaviors of the clamped-clamped porous FGM sandwich beam is investigated in this paper, from which several conclusions can be drawn.

1. The critical temperature of FGM sandwich beams predicted by the theory based on the physical neutral plane is nearly equal to that based on the geometrical middle plane.
2. Neglecting the temperature-dependence of the constituent materials would overestimate the actual critical temperature. Meanwhile, an approximation of the actual thermal environment by a linear temperature rise method would arouse tremendous error and greatly underestimate the prediction of the critical buckling load. Hence, thermal buckling analysis for FGM sandwich beams should take the temperature-dependent material properties and the practical thermal conduction into consideration.
3. The existence of porosity would increase the critical temperatures of FGM sandwich beams, and the uniform porosity distribution (FGM-I) affects more significantly on the increase of critical temperatures than the non-uniform porosity distribution (FGM-II).
4. The critical temperature of the sandwich beam with a smaller face-to-core ratio is more sensitive to the change in the power-law index and the porosity parameter.
5. To improve the thermal buckling load of FGM beams, the ceramic constituent with a lower thermal expansion coefficient would be preferred.

Acknowledgements

This work was supported by the National Natural Science Foundation of China (Grant Nos. 11402093), and the Science and Technology Program of Guangzhou (Grant Nos. 201607010282).

References

[1] Thai Huu-Tai, Kim Seung-Eock. A review of theories for the modeling and analysis of functionally graded plates and shells. Compos Struct 2015;128:70–86.
[2] Bouhadra Abdelhakim, Benyoucef Samir, Tounsi Abdelouahed, Bernard Fabrice, Bouiadjra Rabbab Bachir, Houari Mohammed Sid Ahmed. Thermal buckling response of functionally graded plates with clamped boundary conditions. J Therm Stresses 2015;38(6):630–50.
[3] Trinh Luan C, Vo Thuc P, Thai Huu-Tai, Nguyen Trung-Kien. An analytical method for the vibration and buckling of functionally graded beams under mechanical and thermal loads. Compos B Eng 2016;100:152–63.
[4] She Gui-Lin, Yuan Fuh-Gwo, Ren Yi-Ru. Thermal buckling and post-buckling analysis of functionally graded beams based on a general higher-order shear deformation theory. Appl Math Model 2017;47:340–57.
[5] Zhu Jingchuan, Lai Zhonghong, Yin Zhongda, Jeon Jaeho, Lee Sooyoung. Fabrication of zro2-nicr functionally graded material by powder metallurgy. Mater Chem Phys 2001;68(1–3):130–5.
[6] Wattanasakulpong Nuttawit, Gangadhara Prusty B, Kelly Donald W, Hoffman Mark. Free vibration analysis of layered functionally graded beams with experimental validation. Mater Des 2012;36:182–90.
[7] Wattanasakulpong Nuttawit, Ungbhakorn Variddhi. Linear and nonlinear vibration analysis of elastically restrained ends fgm beams with porosities. Aero Sci Technol 2014;32(1):111–20.
[8] Wattanasakulpong Nuttawit, Chaikittiratana Arisara. Flexural vibration of imperfect functionally graded beams based on timoshenko beam theory: Chebyshev collocation method. Meccanica 2015;50(5):1331–42.
[9] Rjoub Yousef S Al, Hamad Azhar G. Free vibration of functionally euler-Bernoulli and timoshenko graded porous beams using the transfer matrix method. KSCE J. Civ. Eng. 2017;21(3):792–806https://doi.org/10.1007/s1.
[10] Ebrahimi Farzad, Ghasemi Fatemeh, Salari Erfan. Investigating thermal effects on vibration behavior of temperature-dependent compositionally graded euler beams with porosities. Meccanica 2016;51(1):223–49.
[11] Ebrahimi Farzad, Ali Jafari. A higher-order thermomechanical vibration analysis of temperature-dependent fgm beams with porosities. J Eng 2016:1–20. 2016.
[12] Ait Atmane Hassen, Tounsi Abdelouahed, Bernard Fabrice. Effect of thickness stretching and porosity on mechanical response of a functionally graded beams resting on elastic foundations. Int J Mech Mater Des 2017;13(1):71–84.
[13] Barati MR, Sadr MH, Zenkour AM. Buckling analysis of higher order graded smart piezoelectric plates with porosities resting on elastic foundation. Int J Mech Sci 2016;117:309–20.
[14] Zhang Da-Guang, Zhou You-He. A theoretical analysis of fgm thin plates based on physical neutral surface. Comput Mater Sci 2008;44(2):716–20.
[15] Abrate Serge. Functionally graded plates behave like homogeneous plates. Compos B Eng 2008;39(1):151–8.
[16] Prakash T, Singha MK, Ganapathi M. Influence of neutral surface position on the nonlinear stability behavior of functionally graded plates. Comput Mech 2009;43(3):341–50.
[17] Bouiadjra Rabbab Bachir, Adda Bedia EA, Tounsi Abdelouahed. Nonlinear thermal buckling behavior of functionally graded plates using an efficient sinusoidal shear deformation theory. Struct Eng Mech 2013;48(4):547–67.
[18] Bellifa Hichem, Benrahou Kouider Halim, Hadji L, Ahmed Houari Mohammed Sid, Tounsi Abdelouahed. Bending and free vibration analysis of functionally graded plates using a simple shear deformation theory and the concept the neutral surface position. J Braz Soc Mech Sci Eng 2016;38(1):265–75.
[19] Ma LS, Lee DW. A further discussion of nonlinear mechanical behavior for fgm beams under in-plane thermal loading. Compos Struct 2011;93(2):831–42.
[20] Fu Yiming, Wang Jianzhe, Mao Yiqi. Nonlinear analysis of buckling, free vibration and dynamic stability for the piezoelectric functionally graded beams in thermal environment. Appl Math Model 2012;36(9):4324–40.
[21] Zhang Da-Guang. Thermal post-buckling and nonlinear vibration analysis of fgm beams based on physical neutral surface and high order shear deformation theory. Meccanica 2014;49(2):283–93.
[22] Fekrar Abdelkader, Ahmed Houari Mohammed Sid, Tounsi Abdelouahed, Mahmoud SR. A new five-unknown refined theory based on neutral surface position for bending analysis of exponential graded plates. Meccanica 2014;49(4):795–810.
[23] Ebrahimi Farzad, Ali Jafari, Barati Mohammad Reza. Free vibration analysis of smart porous plates subjected to various physical fields considering neutral surface position. Arabian J Sci Eng 2016.
[24] Kim Nam-Il, Lee Jaehong. Geometrically nonlinear isogeometric analysis of functionally graded plates based on first-order shear deformation theory considering physical neutral surface. Compos Struct 2016;153:804–14.
[25] Amir Farzam-Rad S, Hassani Behrooz, Karamodin Abbas. Isogeometric analysis of functionally graded plates using a new quasi-3d shear deformation theory based on physical neutral surface. Compos B Eng 2017;108:174–89.
[26] Reddy JN, Chin CD. Thermomechanical analysis of functionally graded cylinders and plates. J Therm Stresses 1998;21(6):593–626.
[27] Zenkour Ashraf M. Generalized shear deformation theory for bending analysis of functionally graded plates. Appl Math Model 2006;30(1):67–84.
[28] Esfahani SE, Kiani Y, Eslami MR. Non-linear thermal stability analysis of temperature dependent fgm beams supported on non-linear hardening elastic foundations. Int J Mech Sci 2013;69:10–20.